Journal of the Physical Society of Japan **95**, 034802 (2026) **Full Papers**
https://doi.org/10.7566/JPSJ.95.034802

Bimodal Oscillations of Aniline Droplets at the Air–Water Interface: Temperature Dependence and Mode Coupling

Koichiro Sadakane*, Hiroshi Ueno†, and Ryusei Wada

Faculty of Life and Medical Sciences, Doshisha University, Kyotanabe, Kyoto 610-0394, Japan

(Received June 14, 2025; revised December 31, 2025; accepted January 23, 2026; published online February 26, 2026)

The autonomous oscillation of aniline droplets floating at the air–water interface was investigated with a focus on the temperature dependence. Two distinct vibrational modes were identified: a low-frequency mode involving large-scale deformation, and a high-frequency mode exhibiting damped inertial rebound. As the solution temperature increased from 7 to 46 °C, the period of the low-frequency mode decreased significantly, whereas that of the high-frequency mode remained nearly constant (0.5–0.6 s). In particular, the results suggest that at high temperatures, high-frequency modes may act as a phase-locking cue, inducing the onset of low-frequency deformation. At 46 °C, the two modes converged in period and amplitude, resulting in a unified oscillatory state. These findings suggest the coexistence of two different oscillation modes, that is, Marangoni-driven and inertia-based oscillations, and that these two modes exhibit different temperature dependences. This study provides fundamental insights into the non-equilibrium vibrational phenomena arising from interfacial instability, offering a simple model system for thermally tunable self-organized behaviors.

1. Introduction

Morphological changes and self-propulsion in biological cells are prominently manifested in phenomena such as cytoskeletal remodeling, membrane extension, and cell division, all of which are active processes maintained under non-equilibrium conditions driven by chemical energy.[1,2] In recent years, the autonomous motion and oscillation of inanimate droplets have attracted significant attention as model systems that mimic biological phenomena in the interdisciplinary fields of soft matter physics and biophysics.[3–5] Droplet motions driven by interfacial Marangoni effects, arising from spatial inhomogeneities in surface tension caused by gradients in concentration, temperature, or chemical reactions, are particularly useful for understanding the fundamental principles of self-organization and autonomy, as they exhibit spontaneous motion and oscillation without external energy input.[6–14]

Such droplet systems have been shown to exhibit various spatiotemporal dynamics, including periodic, quasi-periodic, and chaotic fluctuations, which are similar to those of reaction diffusion systems and nonlinear oscillators.[15] Furthermore, it has been reported that multiple oscillating droplets can synchronize through Marangoni convection or diffusional coupling, a behavior analogous to the assemblies of chemical oscillators or pacemaker systems in biological rhythms.[16–18] Thus, these oscillatory droplet systems provide a promising platform for studying self-organization and coordinated motion in open non-equilibrium systems and may ultimately contribute to the design of artificial life systems.[19–22]

In our previous study, we investigated autonomous shape oscillations and synchronization phenomena of aniline droplets floating on a water surface.[23] We clearly observed and analyzed the synchronization induced by interactions among the droplets, and demonstrated that aniline droplets undergo spontaneous, periodic expansion-contraction motions. Moreover, we demonstrated that multiple droplets interact via Marangoni convection and surface tension gradients, leading to synchronized oscillations. Numerical simulations supported these findings by proposing a mechanism in which time-dependent surface tension variations are driven by Marangoni flows, and confirmed that the onset of synchronization depends on the inter-droplet distance.

In the present study, we performed a more detailed quantitative analysis of the oscillatory behavior of droplets discovered in our previous work.[23] To enable precise observation, we placed aniline droplets in a cylindrical glass bottle with an inner diameter comparable to the droplet size to suppress the influence of diffusion. Recognizing that temperature affects key physical properties, such as the diffusion coefficient and interfacial tension, we systematically examined the influence of temperature variations on the oscillation modes of the droplets. As demonstrated in our previous study,[23] the oscillatory characteristics of aniline droplets are sensitive to the droplet size and the geometrical configuration of the chamber. Specifically, it has been reported that the oscillation period increases with the droplet size. In addition, increasing the depth of the aqueous phase beneath the floating droplet, which effectively modifies the hydrodynamic environment, leads to a decrease in the oscillation period. In contrast, the lateral surface area of the chamber was found to have only a minor influence on the oscillatory behavior. Accordingly, these geometrical parameters were fixed, and the experiments were designed to focus exclusively on the temperature-induced modification of the oscillation modes under well-defined and controlled conditions.

2. Experiments

To investigate the temperature dependence of the autonomous oscillations of aniline droplets, we constructed an experimental apparatus, as illustrated in Fig. 1. The system was built around a thermostatic water bath that was capable of precise temperature control. Specifically, a square glass tank (outer dimensions: $195 \times 195\,\mathrm{mm}^2$) was filled with thermal bath water, and a cylindrical stainless-steel container (inner diameter: 100 mm) was placed at the center of the tank. The stainless-steel container was heated by circulating water to reach the desired temperature. The heat was then transferred via the surrounding thermal bath water to a cylindrical glass bottle (inner diameter: 24.5 mm, height:

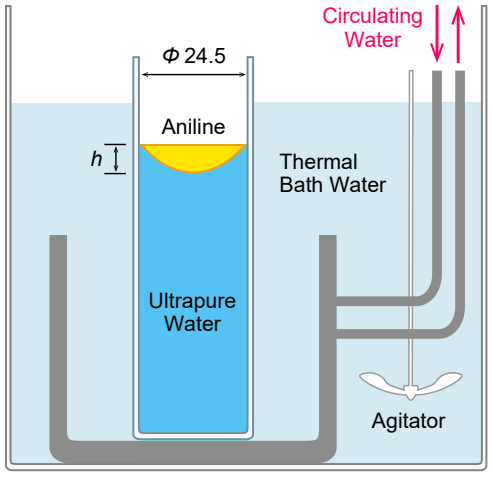

Fig. 1. (Color online) Schematic illustration of the experimental apparatus. A cylindrical stainless-steel container, in which the circulating water is temperature-controlled, is placed at the center of a square glass water tank filled with thermal bath water. A cylindrical glass bottle (inner diameter: 24.5 mm, height: 140 mm) containing the sample is placed at the center of the stainless-steel container. The entire system is uniformly heated by stirring in thermal bath water using an agitator. An aniline droplet floats on the water surface inside the glass bottle, and the water depth from the bottom of the droplet to the bottom of the container is approximately 140 mm. The symbol h represents vertical displacement from the water surface to the apex of the aniline droplet.

140 mm) positioned at the center. To ensure uniform temperature distribution, the thermal bath water in the tank was continuously stirred using an agitator. The measured temperature variation around the cylindrical glass bottle was within ±0.2 °C, indicating sufficient thermal uniformity across the observation area. External agitation was halted during video acquisition to avoid mechanical vibrations. It was confirmed that the temperature fluctuations remained within ±0.5 °C. In this manner, temperature control was conducted in the range of 7–46 °C, with a precision of ±0.5 °C. Note that experiments above 46 °C were avoided because aniline rapidly dissolved into the aqueous phase, making it difficult to maintain a stable droplet at the interface.

Aniline (purity: 99.0%) used in the experiments was obtained from Fujifilm Wako Pure Chemical, and ultrapure water was prepared using a Direct-Q3UV system (Merck). The experimental procedure is as follows: First, 40 mL ultrapure water was poured into a glass bottle and allowed to sit in a heat bath for 1 h until equilibrium was reached. Next, a small amount of aniline, which was placed in a heat bath for 1 h, was gently dripped onto the surface of the water using a micropipette. The total volume of aniline floating on the surface of the water was 400 µL. The droplet diameter was adjusted to approximately 24.5 mm of the inner diameter of the glass bottle, and care was taken to maintain this size constant under different temperature conditions. Immediately after the deposition, the aniline droplet floated on the surface and began to exhibit spontaneous vertical oscillations within several tens of seconds. As shown in Figs. 2 and 3, a black shadow is reflected horizontally against the aniline droplet. This is a reflection of the stainless-steel container installed at the bottom of the glass bottle containing the sample. This shadow makes it easier to understand the vibration of the droplet; therefore, it was deliberately reflected in this study. After confirming that the oscillations had reached a steady state, we designated the onset of image acquisition as time $t = 0$ s, and analyzed the portion in which oscillatory motion was clearly sustained (e.g., approximately 140 s at 7 °C and 49 s at 46 °C). This reduction in the oscillation lifetime with increasing temperature is attributed to the accelerated dissolution of aniline into the aqueous phase, which limits the duration over which a well-defined droplet interface can be maintained. Nonetheless, within these time ranges, we confirmed that the value of h reflecting the droplet size remained virtually unchanged (Figs. 2–4). Videos were recorded using an iPhone 11, converted into uncompressed AVI format at 30 fps using AviUtl software, and subsequently analyzed using ImageJ and Igor Pro 9. The temporal evolution of the vertical displacement h of the droplet was quantitatively evaluated.

3. Results and Discussion

Figure 2 illustrates the autonomous oscillation behavior of an aniline droplet observed at a solution temperature of 7 °C. In this study, we focused on the vertical deformation of a droplet and quantitatively analyzed its temporal evolution. Here, x denotes the vertical coordinate measured downward from the water surface, and h represents the vertical displacement from the water surface to the apex of the droplet. Figure 2(a) shows a sequence of still images extracted from a side-view video recording of the droplet, capturing its oscillatory behavior between 4.90 and 5.91 s. From 4.90 to 5.31 s, the droplet exhibits significant vertical elongation. Here we refer this large deformation with short-period as the "low-frequency mode", which is previously reported to be a large-shape oscillation of the droplet.[23] Immediately afterward, the droplet undergoes repeated contraction and re-elongation, which is attributed to damped oscillations arising as a reactive response to the large deformation. We refer this damped oscillation with short-period as the "high-frequency mode". Figure 2(b) shows a spatiotemporal image constructed by aligning the time-series images of the central region of the droplet, providing a visual representation of the shape evolution over time. Figure 2(c) displays the temporal variation of h over a 20 s interval, estimated from the spatiotemporal image. Figure 2(d) extends this analysis to a full 140 s duration.

These data clearly reveal the presence of two distinct oscillation modes, each characterized by a specific timescale. The low-frequency mode exhibits a mean period of $t_L = 9 \pm 4$ s, corresponding to large-scale vertical elongations of the entire droplet. The maximum deformation amplitude during the low-frequency mode is 2.5 ± 0.5 mm. Immediately following each elongation, the high-frequency mode appears as damped oscillations with a consistent period of $t_H = 0.6 \pm 0.1$ s. This temporal sequence, i.e., elongation followed by damped rebound, is representative of the oscillatory behavior at 7 °C, as shown in Figs. 2(c) and 2(d).

The oscillatory behavior of an aniline droplet at a solution temperature of 36 °C is shown in Fig. 3. Figure 3(a) presents a series of still images extracted from a side-view video of the droplet, taken between $t = 0.20$ and 1.13 s. From 0.20 to 0.60 s, the droplet undergoes a large vertical elongation, followed by repeated contraction and re-elongation between

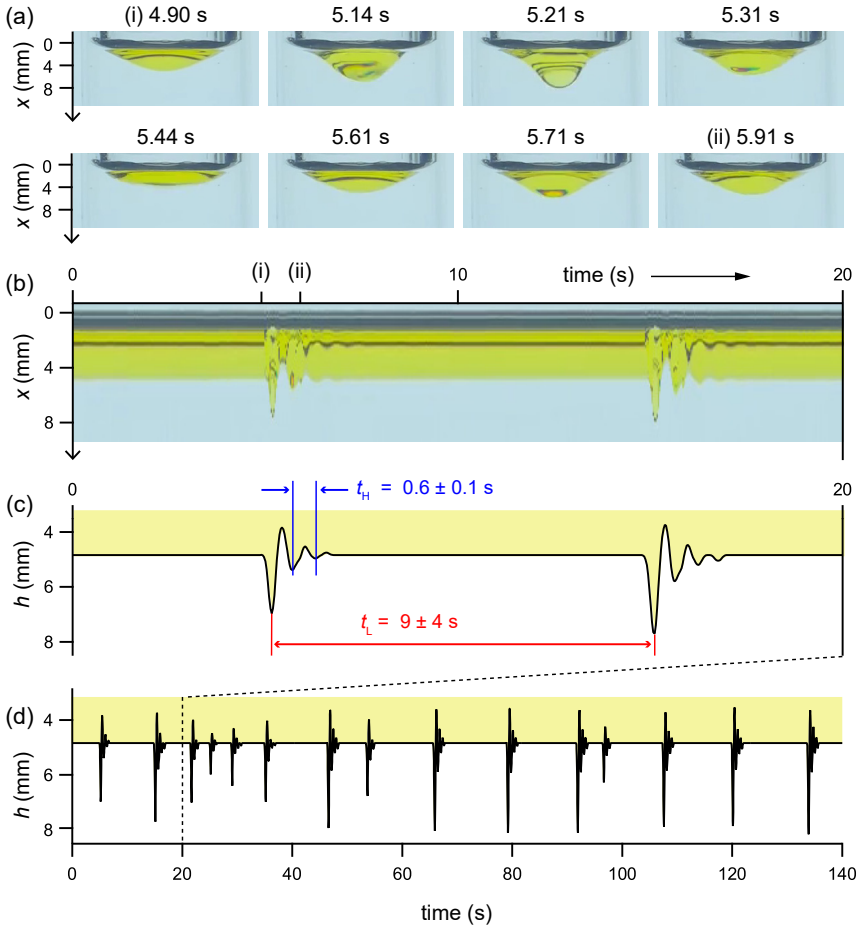

Fig. 2. (Color online) The autonomous oscillation of an aniline droplet observed at a solution temperature of 7 °C. The vertical coordinate x is defined downward from the water surface, and h denotes the vertical displacement from the water surface to the apex of the droplet. (a) Sequence of still images extracted from side-view video recording of droplet. (b) Spatiotemporal image constructed by extracting and aligning the central portion of the droplet over a 20 s time window. Dashed lines (i) and (ii) correspond to the times indicated in (a): 4.90 and 5.91 s, respectively. (c) Temporal variation of h estimated from the spatiotemporal image in (b), showing the presence of two distinct oscillation modes: a low-frequency mode with $t_L = 9 \pm 4$ s and a high-frequency mode with $t_H = 0.6 \pm 0.1$ s. (d) Overall time evolution of h over a 140 s recording.

0.60 and 1.13 s. These behaviors can be understood, as in the case of 7 °C shown in Fig. 2, in terms of two distinct oscillation modes: a low-frequency mode associated with a large deformation and a high-frequency mode that arises as a reactive rebound. Figure 3(b) shows a spatiotemporal image generated by extracting and stacking the central region of the droplet from the video frames over a 20 s interval, thereby visualizing its time evolution. The corresponding temporal variation of h estimated from the spatiotemporal image is shown in Fig. 3(c), and the complete behavior over a 140 s recording is shown in Fig. 3(d). The low-frequency mode has a period of $t_L = 1.5 \pm 0.3$ s, whereas the high-frequency mode has a period of $t_H = 0.50 \pm 0.10$ s. The maximum deformation amplitude during the low-frequency mode is 0.18 ± 0.08 mm, which is substantially smaller than that observed at 7 °C (2.5 ± 0.5 mm).

A noteworthy observation is that, at this temperature, the next low-frequency deformation begins before the preceding high-frequency damped oscillation has fully decayed. Because t_L/t_H is approximately 3, it can be inferred that each low-frequency oscillation is followed by approximately two high-frequency oscillations, and the third high-frequency cycle coincides with the onset of the next large deformation. This evidence indicates that the high-frequency mode may act as a phase-locking cue that promotes the onset of low-frequency deformation.

Figure 4 shows the oscillatory behavior of an aniline droplet at solution temperatures of 24, 42, and 46 °C. Each plot presents a representative 8 s time series of the vertical displacement h under the corresponding temperature conditions. At 24 °C, similar to the behavior observed at 7 °C in Fig. 2, the droplet exhibits a clearly defined low-frequency mode with a period of $t_L = 8 \pm 3$ s, followed immediately by damped high-frequency oscillations with a period of $t_H = 0.50 \pm 0.04$ s. In this case, the high-frequency mode fully decays before the next low-frequency oscillation begins, indicating that the two modes are temporally well-separated. In contrast, at 42 °C, as with the behavior at 36 °C shown in Fig. 3, the next low-frequency deformation begins before the preceding high-frequency oscillation has fully decayed. The periods are evaluated as $t_L = 0.8 \pm 0.1$ s and $t_H = 0.45 \pm 0.06$ s, giving a ratio close to 2. This suggests that the low-frequency mode is re-initiated in synchronization with every first or second cycle of the high-frequency mode. The relative error of t_L (0.1/0.8 = 0.125) is smaller than that at 36 °C, implying further enhancement in periodic stability. These findings indicate that the high-frequency mode may serve more clearly as a phase-locking cue that induces the onset of

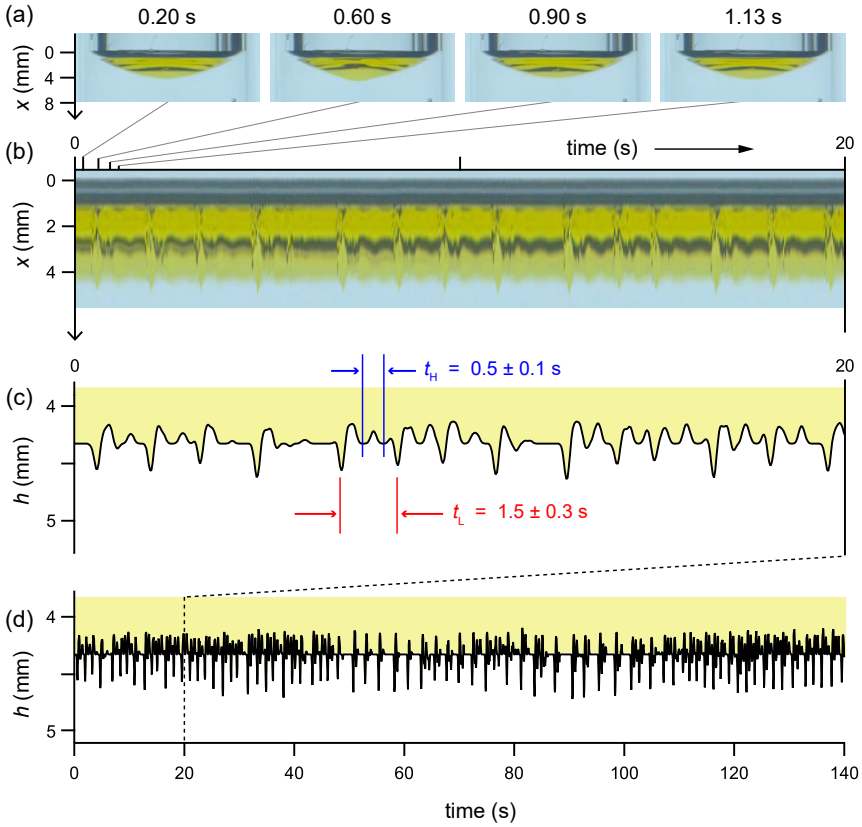

Fig. 3. (Color online) The autonomous oscillation of an aniline droplet observed at a solution temperature of 36 °C. The vertical coordinate x is defined downward from the water surface, and h denotes the vertical displacement from the water surface to the apex of the droplet. (a) Still images extracted from a side-view video recording of the droplet from $t = 0.20$ to 1.13 s. (b) Spatiotemporal image showing the temporal evolution of the droplet shape over a 20 s duration, constructed by aligning the central region of the droplet from sequential video frames. (c) Temporal variation of h estimated from (b). (d) Time evolution of h over the entire 140 s recording. Repeated excitation of high-frequency damped oscillations following each low-frequency elongation is clearly evident.

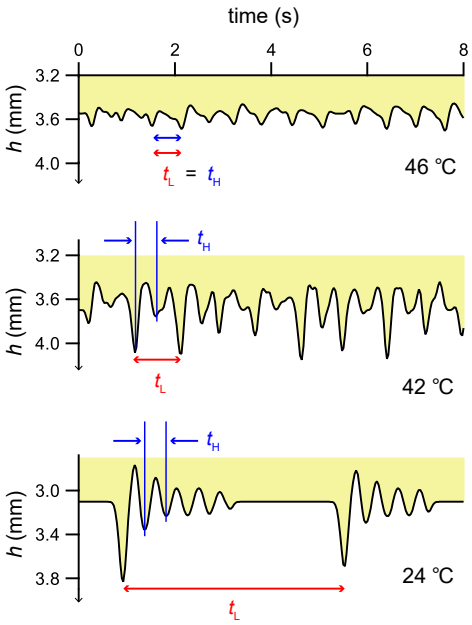

Fig. 4. (Color online) Time evolution of the vertical displacement h of aniline droplets observed at solution temperatures of 24, 42, and 46 °C. Each plot presents an 8 s representative time series of h at the respective temperatures. t_L and t_H denote the periods of the low- and high-frequency oscillation modes, respectively. At 46 °C, the two modes appear to have merged, and are therefore represented as $t_L = t_H$.

the low-frequency mode. A rigorous quantitative assessment of this coupling mechanism, such as the statistical analysis of phase differences or time delays between two modes, remains an important topic for future investigations.

When the temperature is increased to 46 °C, the amplitude of the low-frequency mode becomes markedly smaller, and its period also shortens, making it difficult to distinguish from the high-frequency mode. At this temperature, the oscillation period is evaluated as $t_L = t_H = 0.63 \pm 0.06$ s, and the distinction between the two modes is effectively lost. The droplet appears to sustain continuous high-frequency oscillations with a stable rhythm, and no clear traces of the low-frequency mode are observed.

These results demonstrate that, with increasing temperature, the period and amplitude of the low-frequency mode decrease, whereas the period of the high-frequency mode remains nearly unchanged. Under high-temperature conditions, the two modes gradually merge, and the droplet transitions into a state of continuous oscillation with a single characteristic period.

Based on the above results, we quantitatively analyzed the oscillation modes of the droplets by performing a fast Fourier transform (FFT) on the temporal evolution of h and evaluating the resulting amplitude spectra. Figure 5 shows FFT spectra obtained under various temperature conditions. The horizontal axis represents the frequency (Hz), and the vertical axis represents the corresponding spectral amplitude.

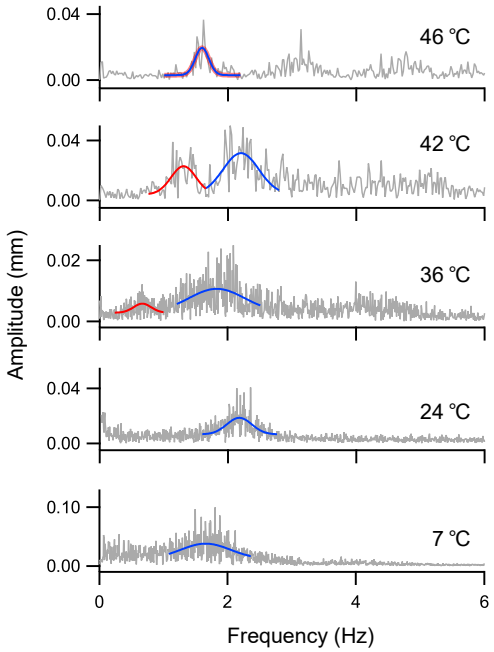

Fig. 5. (Color online) Amplitude spectra obtained by applying Fourier transform to the time evolution of the vertical displacement h of an aniline droplet. The horizontal axis represents frequency (Hz), and the vertical axis indicates the corresponding spectral amplitude. Each curve corresponds to a different temperature condition. To clarify the peak positions, each peak arising from the low- and high-frequency modes are traced by a fitting curve with a Gaussian function: the red and blue curves correspond to the low- and high-frequency modes, respectively. At 46 °C, the two peaks converge into a single peak around 1.6 Hz, accompanied by observable higher harmonic components.

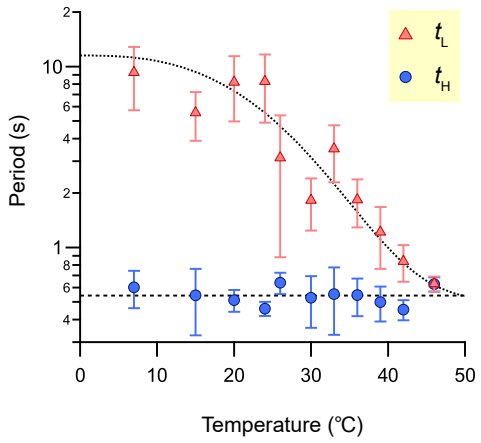

Fig. 6. (Color online) Temperature dependence of the oscillation periods of the low-frequency mode t_L and high-frequency mode t_H observed in the aniline droplets. The filled triangles represent t_L, whereas the filled circles represent t_H. The error bars indicate the standard deviation of the measured periods. The dashed line represents the average period of the high-frequency mode (0.54 s), and the dotted line serves as a visual guide illustrating the decreasing trend of t_L with increasing temperature.

To clarify the peak positions, each peak arising from the low- and high-frequency modes are traced by a fitting curve with a Gaussian function: the red and blue curves correspond to the low- and high-frequency modes, respectively. At 7 and 24 °C, distinct peaks corresponding to the high-frequency mode are evident, whereas peaks corresponding to the low-frequency mode are not clearly observed. On the other hand, the spectra at 36 and 42 °C show well-defined peaks corresponding to both the low- and high-frequency modes. In particular, the peak associated with the low-frequency mode at 42 °C is more pronounced than that at 36 °C, which is consistent with the observation in Fig. 4 that the oscillation becomes more stable and regular at higher temperatures. Furthermore, at 46 °C, the periods of the low- and high-frequency modes converge, resulting in a single peak appearing around 1.6 Hz. Higher harmonic components are also observed at higher frequencies, indicating that the droplet maintains continuous oscillations with a stable rhythm. These results suggest that, under high-temperature conditions, the two distinct oscillation modes merge and transition into a unified oscillatory state.

Figure 6 shows the temperature dependence of the oscillation periods for the low-frequency mode (t_L) and high-frequency mode (t_H) observed in aniline droplets. The values of t_L were obtained through time-domain analysis of the full time course of the droplet apex height h. The associated error bars represent the standard deviations of the measured periods. By contrast, t_H was determined from the peak positions of the Gaussian fits applied to the amplitude spectra shown in Fig. 5, with the error bars indicating the standard deviation of each fitted Gaussian. As shown in Fig. 6, t_L exhibits a monotonic decrease with increasing temperature, showing a particularly steep decline between 7 and 42 °C. In contrast, t_H remains nearly constant within the range of 0.5–0.6 s, showing no clear temperature dependence.

Herein, we discuss the physical origins of the observed oscillation modes and their temperature dependence. The decreasing trend of t_L can be naturally interpreted in light of our previous study,[23] which identified the low-frequency mode as being driven by Marangoni convection. As the temperature increases, the diffusion coefficient of aniline increases, resulting in steeper and more dynamic concentration gradients near the droplet interface. This, in turn, accelerates both the onset and decay of Marangoni flow. As a result, the interfacial tension gradients that drive the large-scale deformation of the droplet become more frequent, thereby shortening the oscillation period.

On the other hand, the near-constant value of t_H across the entire temperature range suggests that the high-frequency mode is not governed by the Marangoni flow, but rather arises from inertial and viscous effects within the droplet. Specifically, this mode appears to be a damped inertial response that follows the large deformation induced by the low-frequency mode. To examine the physical origin of the high-frequency mode more quantitatively, we estimated the characteristic inertio-capillary timescale τ based on dimensional analysis. The timescale is given by:

$$\tau \sim \sqrt{\frac{\rho R^3}{\gamma}}, \tag{1}$$

where ρ is the density of the droplet, R is the droplet radius, and γ is the interfacial tension between the aniline and water.[24,25] The density of aniline is reported to be 1021 kg/m^3 at 20 °C,[26] and is assumed to vary negligibly between 7 and 46 °C. Similarly, the interfacial tension between aniline and water is 5.8 mN/m at 20 °C,[27] and is assumed to remain approximately constant in the same temperature range. The radius of the floating droplet was estimated to be $R = 12$ mm based on the geometry of the cylindrical container shown in

Fig. 1 (with an inner diameter of 24.5 mm). Substituting these values into Eq. (1) yields $\tau \approx 0.55$ s. This estimated value agrees well with the experimentally observed period of the high-frequency mode (approximately 0.5–0.6 s), strongly supporting the interpretation that this mode originates from mechanical oscillation governed by the balance between interfacial tension and inertia.

Finally, we examined several secondary factors that could potentially influence the oscillatory behavior of aniline droplets beyond the temperature effects discussed above. As aniline is a weak base with a reported pKb of approximately 9.3, aniline dissolved in water is expected to render the aqueous phase weakly alkaline through partial protonation. To examine how changes in the protonation state of aniline affect interfacial instability and oscillatory behavior, we intentionally shifted the aqueous phase to weakly acidic conditions.

Specifically, the influence of pH was examined by floating an aniline droplet on an aqueous solution prepared by adding 1.5 mL of acetic acid to 38.5 mL of water, resulting in a pH of approximately 2.5. Under these acidic conditions, the aniline droplet rapidly dissolved into the aqueous phase, and no sustained oscillatory motion was observed. This behavior suggests that significant protonation of aniline suppresses the interfacial instability required for oscillation. Because changing the pH substantially alters the chemical nature of aniline, a systematic investigation of the pH effects without simultaneously modifying the interfacial chemistry is experimentally difficult. Nevertheless, Marangoni-driven interfacial instabilities have also been reported for chemically neutral systems, such as nitrobenzene droplets. This comparison suggests that the emergence of interfacial instability is not directly governed by pH but rather by the balance between interfacial tension gradients, dissolution, and hydrodynamic response.

In addition, the influence of evaporation was examined by performing control experiments under the same conditions as those shown in Fig. 2, but with the cylindrical glass bottle covered. Under these conditions, no noticeable changes were observed in the oscillation period, amplitude, or duration. Furthermore, as described above, the value of apex height h, which reflects droplet size, remained nearly constant while oscillations persisted. These observations indicate that evaporation does not significantly affect the oscillatory characteristics of the system.

As a future research, we should also discuss the phenomenon of vibration synchronization. Although the present study focused on the temperature-dependent oscillatory behavior of a single aniline droplet, the findings also provide insight into the potential collective behaviors in systems of multiple droplets. Our previous work[23] demonstrated that an ensemble of droplets can exhibit spontaneous synchronization via Marangoni-induced interfacial coupling, particularly when droplets are placed within a few centimeters of each other. The distinction between the temperature-sensitive low-frequency mode and the robust high-frequency mode suggests that the latter may serve as a phase reference or timing cue in a collective context. This raises the possibility that high-frequency oscillations can mediate synchronization among droplets even when low-frequency modes vary across individuals. Future studies extending this framework to multiple-droplet systems will be valuable for elucidating nonlinear collective dynamics in interfacial systems.

4. Conclusion

In this study, we investigated the autonomous oscillatory behavior of aniline droplets floating at the air–water interface, with a particular focus on its temperature dependence. In addition to the low-frequency mode involving large-scale deformation reported in our previous work, we newly identified a short-period damped oscillation mode, referred to as the high-frequency mode. These findings reveal that the oscillations of aniline droplets consist of two distinct vibrational modes characterized by different temporal scales. By systematically varying the temperature of the aqueous phase, we observed significant changes in both periods and in the interrelation between the two modes. Specifically, the period of the low-frequency mode decreased with increasing temperature, whereas that of the high-frequency mode remained nearly constant at approximately 0.5–0.6 s. This result suggests that the low-frequency mode is driven by Marangoni convection, whereas the high-frequency mode originates from inertial-capillary oscillations. The latter interpretation is supported by a dimensional estimate yielding a characteristic timescale of 0.55 s, which agrees well with the observed period. At elevated temperatures, the high-frequency mode appears to function as a phase-locking cue that promotes the onset of the low-frequency deformation. At the highest temperature investigated (46 °C), the two modes became nearly indistinguishable in both period and amplitude, indicating a transition to a unified oscillatory state.

These results demonstrate that a simple droplet system, such as aniline, at the air–water interface can exhibit nonlinear dynamic behavior involving the coexistence, interaction, and merging of multiple oscillatory modes under external thermal control. This study provides a new quantitative perspective on interfacial oscillations by successfully disentangling and characterizing two distinct vibrational modes in a minimal single-droplet system. The coexistence and interaction of Marangoni-driven and inertia-based oscillations reveal a previously unexplored dynamical regime, offering a valuable framework for future investigations into spontaneous pattern formation and collective dynamics in non-equilibrium soft matter systems. Furthermore, such systems may serve as useful models for exploring thermally responsive behaviors and self-organization processes in soft matter and biological contexts.

Acknowledgment The authors thank Professor Yoshikawa at Doshisha University for valuable discussions. HU wishes to acknowledge the support provided by the Yoshida Scholarship Foundation for the "Doctor 21" program.

*ksadakan@mail.doshisha.ac.jp
†uaeneau@dmpl.doshisha.ac.jp

1) T. Toyota, N. Maru, M. M. Hanczyc, T. Ikegami, and T. Sugawara, J. Am. Chem. Soc. **131**, 5012 (2009).
2) M. C. Marchetti, Nature **491**, 340 (2012).
3) C. C. Maass, C. Krüger, S. Herminghaus, and C. Bahr, Annu. Rev. Condens. Matter Phys. **7**, 171 (2016).
4) M. M. Hanczyc, T. Toyota, T. Ikegami, N. Packard, and T. Sugawara, J. Am. Chem. Soc. **129**, 9386 (2007).
5) D. Okawa, S. J. Pastine, A. Zettl, and J. M. Fréchet, J. Am. Chem. Soc. **131**, 5396 (2009).

6) M. Schmitt and H. Stark, Phys. Fluids **28**, 012106 (2016).
7) K. Nagai, Y. Sumino, and K. Yoshikawa, Colloids Surf. B **56**, 197 (2007).
8) M. P. Stewart, J. Helenius, Y. Toyoda, S. P. Ramanathan, D. J. Muller, and A. A. Hyman, Nature **469**, 226 (2011).
9) M. C. Marchetti, J.-F. Joanny, S. Ramaswamy, T. B. Liverpool, J. Prost, M. Rao, and R. A. Simha, Rev. Mod. Phys. **85**, 1143 (2013).
10) Y.-J. Chen, Y. Nagamine, and K. Yoshikawa, Phys. Rev. E **80**, 016303 (2009).
11) S. Sato, H. Sakuta, K. Sadakane, and K. Yoshikawa, ACS Omega **4**, 12766 (2019).
12) S. A. Shenoy, K. Chaithanya, and P. Dayal, Soft Matter **21**, 1957 (2025).
13) A. Shundo, K. Mizuguchi, M. Miyamoto, M. Goto, and K. Tanaka, Chem. Commun. **47**, 8844 (2011).
14) T. Furuki, H. Sakuta, N. Yanagisawa, S. Tabuchi, A. Kamo, D. S. Shimamoto, and M. Yanagisawa, ACS Appl. Mater. Interfaces **16**, 43016 (2024).
15) C. Lv, C. Chen, Y.-C. Chuang, F.-G. Tseng, Y. Yin, F. Grey, and Q. Zheng, Phys. Rev. Lett. **113**, 026101 (2014).
16) Y. Sumino, N. Magome, T. Hamada, and K. Yoshikawa, Phys. Rev. Lett. **94**, 068301 (2005).
17) M. Leoni and T. Liverpool, Phys. Rev. Lett. **112**, 148104 (2014).
18) P. B. Duncan and D. Needham, Langmuir **22**, 4190 (2006).
19) I. Nitsan, S. Drori, Y. E. Lewis, S. Cohen, and S. Tzlil, Nat. Phys. **12**, 472 (2016).
20) N. Kovalchuk and D. Vollhardt, J. Phys. Chem. C **112**, 9016 (2008).
21) R. Stocker and J. W. Bush, J. Fluid Mech. **583**, 465 (2007).
22) B. Haller, K. Jahnke, M. Weiss, K. Göpfrich, I. Platzman, and J. P. Spatz, Adv. Intell. Syst. **3**, 2000190 (2021).
23) Y.-J. Chen, K. Sadakane, H. Sakuta, C. Yao, and K. Yoshikawa, Langmuir **33**, 12362 (2017).
24) L. Rayleigh, Proc. R. Soc. Lond. **29**, 71 (1879).
25) A. Potnis and A. Saha, J. Fluid Mech. **988**, A15 (2024).
26) S. Patil, A. Chaudhari, M. Lokhande, M. Lande, A. Shankarwar, S. Helambe, B. Arbad, and S. Mehrotra, J. Chem. Eng. Data **44**, 875 (1999).
27) L. A. Girifalco and R. J. Good, J. Phys. Chem. **61**, 904 (1957).